Impact of the pre amorphization by Ge implantation on Ni_0.9Pt_0.1 silicide

C. Delwail, S. Joblot, F. Mazen, F. Abbate, L. Lachal, F. Milesi, M. Bertoglio, A.M. Papon, M. Gregoire, P.H. Rodriguez, et al.

Impact of the pre amorphization by Ge implantation on $Ni_{0.9}Pt_{0.1}$ silicide

C. Delwail[abc*], S. Joblot[a], F. Mazen[b], F. Abbate[a], L. Lachal[b], F. Milesi[b], M. Bertoglio[c], AM Papon[b], M. Grégoire[a], Ph. Rodriguez[b] and D. Mangelinck[c]

[a] *STMicroelectronics, 850 rue Jean Monnet, 38926 Crolles Cedex, France*

[b] *Univ. Grenoble Alpes, CEA, LETI, F-38000 Grenoble, France*

[c] *IM2NP, CNRS, Aix-Marseille Université, faculté de saint Jérôme, 13397 Marseille Cedex 20, France*

Abstract

The impact of the Pre Amorphization by Ge Implantation (PAI) on $Ni_{0.9}Pt_{0.1}$ silicide is studied. Reactions between a 10 nm thick $Ni_{0.9}Pt_{0.1}$ film and Si (100) substrate are analyzed as a function of the induced amorphous thicknesses. In view of being compatible with the integration constraint of the 28 nm CMOS technologies, the Ge implantation dose is fixed at a low level. The relative position of the amorphous/crystalline interface and the silicide growth front is defined for each sample. Then, in-situ XRD analyses, X-Ray Reflectometry (XRR) and Sheet resistance (Rs) measurements are achieved to provide a deep study of silicide growth kinetics and silicide properties. First, a clear relationship is established between the silicide growth rate and the amorphous thickness. Secondly, an easier NiSi nucleation and a decrease of its resistivity is observed when NiSi nucleates at the θ-Ni_2Si/a-Si interface. These observations are discussed considering the impact of the amorphous layer on the driving force, the nucleation barrier, the lateral growth rate, and NiSi roughness.

Keywords

$Ni_{0.9}Pt_{0.1}$ silicide, PAI, Kinetics, Resistivity

1. Introduction

Silicides are obtained by solid state reaction between a thin metal film and a Si substrate. In microelectronics devices and more precisely for technology nodes below 65 nm, the Ni silicide is the preferred material because of its low resistivity, low thermal budget and low silicon consumption required for the NiSi formation [1]. Nevertheless, the NiSi has two major drawbacks. First, the NiSi phase is no longer stable after 600°C due to agglomeration issues. Then, from 750°C, the resistive $NiSi_2$ phase nucleates at the expense of the NiSi. These issues are partly solved with the addition of Pt to the Ni. Thereby, the Pt alloyed to the Ni allows to extend the thermal stability up to 900°C from 40 nm thick silicides [2], without drastically changes the Ni-silicides advantages. In addition, Detavernier et al. report that the addition of Pt to the Ni reduces the importance of the axiotaxy between the NiSi and the Si. This modification of the texture is assumed to reduce the agglomeration [3]. Consequently, for 28 nm FDSOI technologies node devices, the $Ni_{0.9}Pt_{0.1}$ mono silicide is the update contact material [4,5]. $Ni_{0.9}Pt_{0.1}$ silicide phase sequence, kinetics parameters and properties are well studied [6–12]. The reaction between the $Ni_{0.9}Pt_{0.1}$ and the Si results of a sequential growth: the θ-Ni_2Si phase grows first. Then, once the $Ni_{0.9}Pt_{0.1}$ layer is totally consumed, the NiSi phase grows at the expense of the θ-Ni_2Si layer. Finally, the NiSi is consumed at higher temperature by the $NiSi_2$ formation. Even if the thermal stability is improved with the addition of Pt, the agglomeration is still an issue, particularly for thin silicide layers around 10 nm. In previous studies, the Pre-Amorphization of silicon before the silicidation using ion Implantation (PAI) has been intensively employed. Van Stiphout et al. report that the PAI modify the kinetic and the phase sequence of the Ni silicide depending on the implantation parameters [13]. Indeed, for Ar PAI, the NiSi nucleation temperature is reduced. However, for N PAI, the NiSi nucleation temperature is increased with the dose until the phase sequence change. For high doses of N incorporated, the intermediate theta phase is no longer formed, instead an amorphous phase, a-NiSi appears. In addition, an improvement in thermal stability is related to NiSi axiotaxy loss and higher Nitrogen incorporated into the silicide layer. Moreover, Lachal et al. and Ozcan et al. put forward the influence of the amorphous thickness on the silicide properties and kinetics [14,15]. Lachal *et al.* studied the impact of the Ge and Si on the $Ni_{0.9}Pt_{0.1}$ silicides properties. The silicide roughness, the thermal stability and the resistivity are improved. Moreover, a clear dependance with the amorphous thicknesses formed during the implantation is evidenced [14].

These improvements and kinetics changes indicate that the damaged or amorphous silicon has an influence on the silicidation. However, the kinetics and mechanisms related to these changes are not deeply investigated. To continue the work of Lachal et al, we focused on the impact of Ge implantations at several energies to make the amorphous silicon thicknesses vary. Consequently, our main interest is to determine the

position of the amorphous/crystalline interface (a-Si/c-Si interface) compared to the consumed silicon during the first and second annealing from which the θ-Ni_2Si and NiSi phase grows, respectively. The purpose of this work is to study both θ-Ni_2Si and NiSi phases kinetics and properties as a function of the amorphous thickness.

2. Experimental

Two identical series of samples were processed, one in a R&D environment (CEA-Leti) and the second one in a production environment (ST Microelectronics). Minor differences linked to tool-sets differences and variability are expected. As the same results are obtained for both series, the repeatability and robustness of the observations are evidenced. P-type Si (100) blanket wafers with a resistivity of 20-40 Ω.cm were used. Prior to the pre amorphization step, the samples were desoxidized using a HF/HCL solution. Then, Ge implantations were performed in a VIISTA HCP ion implanter. Implantation conditions were chosen to vary the thickness of the amorphous Si (a-Si) between 2 and 15 nm. The implantation parameters needed to reach the targeted a-Si thicknesses were determined by TCAD simulation, with Synopsys Sentaurus process simulator : the analytical model based on experimental fit was used and the a-Si/c-Si interface was set as the depth corresponding to 2E22 cm^{-3} damages. The dose was fixed at 1E14 at/cm² for each sample while the energy varies from 1 to 11 keV. The as implanted samples were then characterized by TEM analyses to control the coherence between the targeted and measured thicknesses. Prior to the $Ni_{0.9}Pt_{0.1}$/TiN deposition, the Si wafers were cleaned by HF/HCL solution and by in situ chemical etch and anneal process (Siconi™ Process [16]). A 10 nm $Ni_{0.9}Pt_{0.1}$ layer and a capping layer of 7 nm thick TiN were then both deposited by magnetron sputtering. In addition to the PAI sample, a sample without PAI is also provided as reference.
The $Ni_{0.9}Pt_{0.1}$/TiN layers deposited on the Si were then submitted to the standard silicidation process. First, a rapid thermal anneal at 230°C for 20s (RTA1) was performed. Then, the unreacted NiPt and TiN capping were removed by wet selective etching. Lastly, a second rapid thermal anneal at 390°C for 30s (RTA2) was performed.

Two sets of samples were prepared: the first set of samples were stopped after the selective etching while the second ones undergone the whole silicidation process (i.e., until RTA2). All samples were characterized by X-Ray Reflectometry (XRR) to determine the silicide thickness. Four-point probe was used to measure the sheet resistance (Rs) and calculate the silicide resistivity.

To estimate the change in phase sequence, two as deposited samples, the reference, and the Ge PAI sample with the thicker amorphous layer, were characterized by in-situ annealing in a Panalytical Empyrean diffractometer (in-situ XRD). The system was configured in symmetrical Bragg-Brentano geometry and the chamber was under vacuum ($10^{-5} - 10^{-6}$ Torr range). The θ-2θ diffractograms were recorded over 2θ range from 25° to 60° during a step-by-step temperature increase of 5°C from 50 to 400°C. Each diffractogram extracted takes 3 minutes at each step.

3. Results

Fig. 1 shows the TEM analysis of the Si substrates after the 5 keV and 11 keV Ge PAI. The thicknesses of the amorphous Si are about 7 nm and 13 nm, respectively. However, the amorphous layer obtained is not perfectly homogenous. Indeed, crystalline pockets are present toward the surface. In addition, the a-Si/c-Si interface is quite rough, and a damage layer of about 2 nm is observed. Table 1 compares targeted and measured thicknesses of the amorphous Si for the different implantation. Despite this effects, the targeted and measured a-Si thicknesses are well fitted by including the thickness of the damaged layer inside the total amorphous one.

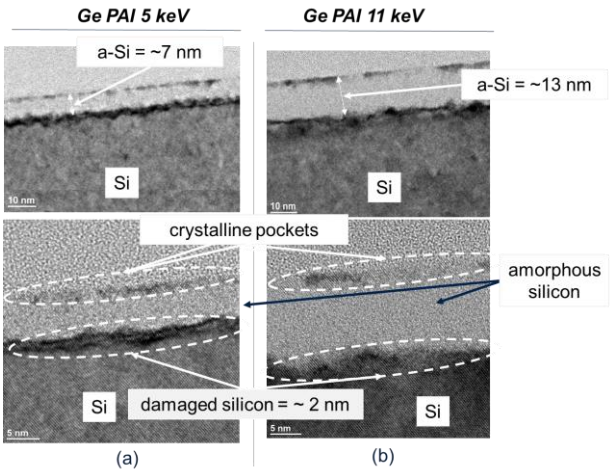

Fig. 1. TEM micrographs of as implanted undoped Si(100), with 1E14 at/cm² Ge PAI (a) 5keV and (b) 11keV for R&D environment samples. Production environment samples show similar results (not shown here)

***Table 1**. a-Si thicknesses according to the implantation parameters*

Ge PAI Tilt : 7° Twist : 27° Dose : 1e14 at/cm²	Energy (keV)	Targeted a-Si thickness (nm)	Measured a-Si thickness (nm)	Measured damaged Si thickness (nm)
	1	2.5	/	/
	3	6	/	/
	5	9	~ 7	~ 2
	7	11	/	/
	9	13	/	/
	11	15	~ 13	~ 2

Fig. 2 shows the in situ XRD measurements for the reference sample without PAI and the sample with the thicker amorphous thickness (Ge PAI with 11 keV, thus all the silicidation occurs inside the a-Si). The XRD peaks intensity are plotted as color level as a function of the temperature and the diffraction angle to follow the reaction between the $Ni_{0.9}Pt_{0.1}$ film and the Si substrate.

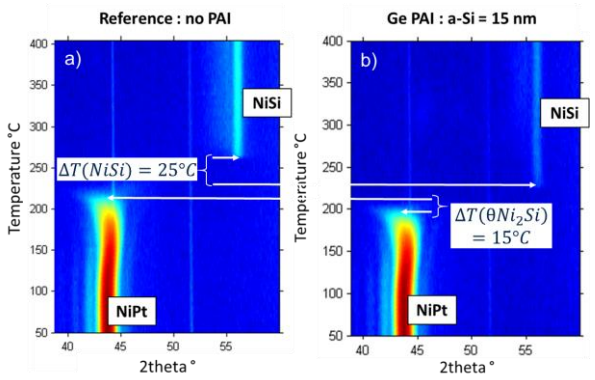

Fig. 2. (Color online) In situ XRD measurements of the reaction of a 10 nm $Ni_{0.9}Pt_{0.1}$ film on Si (100) for a) the reference without PAI and b) the sample with an amorphous thickness of 15 nm corresponding to the 1E14 at/cm² 11keV Ge PAI

For both samples the silicide phase sequence are similar. The θ-Ni_2Si phase grows first by consumption of the NiPt film. Only the decrease of the NiPt peak intensity can be seen in Fig. 2. Therefore, the intermediate phase should be an amorphous phase or the θ-Ni_2Si phase. Indeed, the θ-Ni_2Si phase cannot be seen with the θ/2θ geometry due to the epitaxy of the θ phase on Si (100) [6]. Thus, accordingly to the previous studies about the $Ni_{0.9}Pt_{0.1}$ silicide phase sequence [7–12], the intermediate phase is assumed to be the crystalline θ-Ni_2Si phase. Then, once the NiPt is totally consumed, there is a temperature gap before the NiSi nucleates at the θ/Si interface. Even if the phase sequence is the same, kinetic variations are observed between the two samples: kinetic is faster for the Ge PAI sample compared to the reference. First, the NiPt layer is totally consumed at lower temperature (minus 15°C), which reveals that the θ phase growth rate is enhanced when growing on the a-Si substrate. Then, the NiSi appears at lower temperature (minus 25°C). In addition, the temperature gap between the total consumption of NiPt and the NiSi nucleation is reduced by 15°C. During this gap, the $Ni_{0.9}Pt_{0.1}$ is totally consumed, thus the θ phase is not growing and the NiSi has not begun to nucleate. Such a gap has been reported [17] and was recently attributed to a difficult in nucleation of NiSi by El Kousseifi et al [11]. The lowering of NiSi nucleation temperature for the PAI sample may thus imply that the NiSi nucleation is easier at the θ/a-Si than at the θ/c-Si interface.

The in situ XRD measurements allow to study the silicide phase sequence and kinetics evolution during slow temperature ramps. However, the contact formation in microelectronics has much faster heating rates and shorter times. Therefore, the silicide kinetics and properties will now be analyzed for the two rapid thermal anneals used for the silicide process (RTA1 and RTA2).
Fig. 3 shows the XRR curves of the samples after RTA2 (i.e., when NiSi is formed) for different PAI energies. XRR allows to measure the thickness and the roughness of the silicide layer through the spacing and the magnitude of the oscillations. Fig. 3 clearly shows that the spacing between the oscillations decreases with increasing PAI energy and indicates that the NiSi thickness increases with increasing thickness of a-Si that scales with the PAI energy. This result indicates that the kinetics of silicide formation is enhanced on a-Si. Furthermore, the magnitude of the oscillations slightly decreases with increasing PAI energy. As the roughness is inversely proportional to the magnitude of the oscillation, the NiSi roughness seems to increase qualitatively with the amorphous thickness, but it was difficult to quantify the change in roughness from the curves in Fig. 3. However, the simulation of XRR curves after RTA1 (not shown) and after RTA2 (Fig. 3) samples have allowed to determine the thicknesses of the θ-Ni_2Si and NiSi layers, respectively.

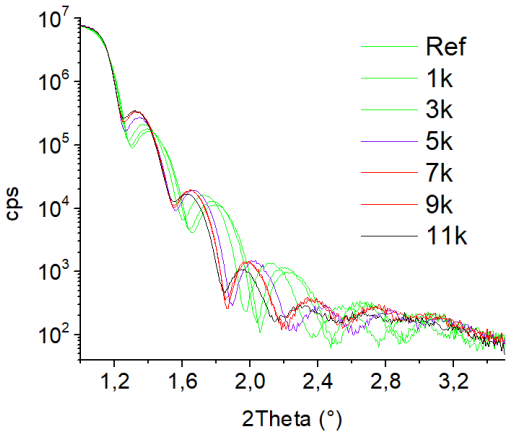

Fig. 3. Evolution of the XRR spectra for the different implantation conditions, Ge PAIs with a dose of 1E14 at/cm², and energies from 1 to 11 keV, corresponding to a-Si thicknesses increasing

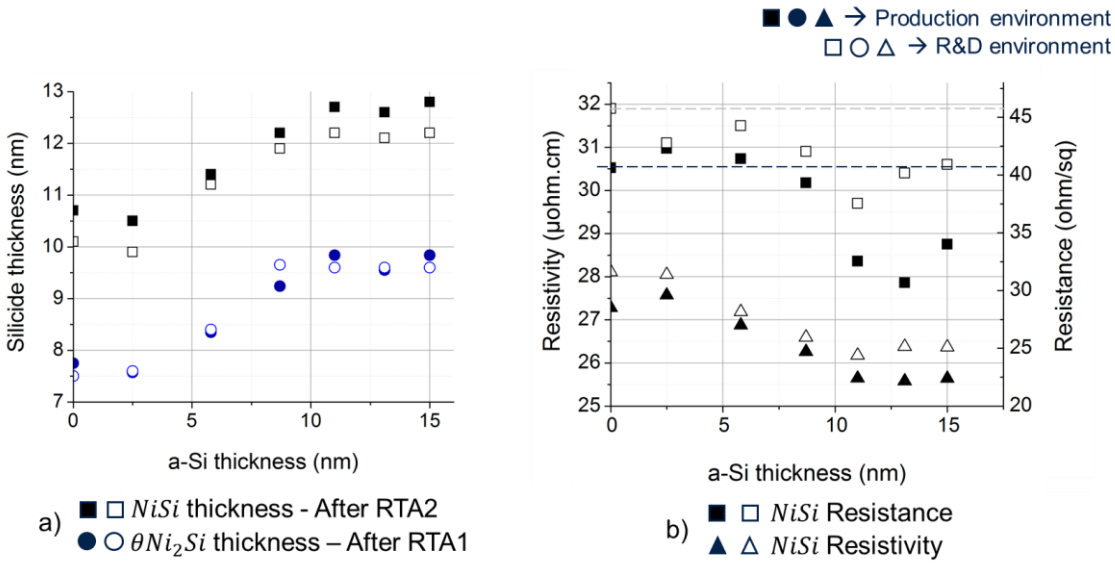

Fig. 4. Evolution of the silicide (a) thickness and (b) resistivity as a function of the a-Si thickness

Fig. 4.a present the θ-Ni_2Si and the NiSi phase thicknesses, respectively formed during the RTA1 and RTA2, that were determined from the XRR measurements. Both NiSi and θ-Ni_2Si thicknesses increase with the a-Si thickness until the silicide thickness reaches a constant level. Fig. 4.a shows also that there is a clear correlation between the thickness of θ-Ni_2Si and the one of NiSi. In fact, this correlation is linked to conservation of matter. Indeed, since the NiPt has been selectively etched before the RTA2, the available amounts of Ni and Pt atoms and thus the NiSi thickness depends only on the θ thickness which grows during the RTA1. In other words, the NiSi thickness corresponds to the whole transformation of θ-Ni_2Si thickness formed during RTA1 into the NiSi phase. Thus, the NiSi thicknesses are not representative of a kinetic variation during the RTA2 but only to the change of kinetics during RTA1. According to the conservation theory of matter, as 10 nm of $Ni_{0.9}Pt_{0.1}$ were deposited on the Si substrates, about 18 nm of the θNi_2Si phase should have been measured if the entire NiPt layer had reacted. As the silicide thicknesses measured are far less than 18 nm, the NiPt layer was not fully consumed regardless of the amorphous thicknesses. Consequently, as the thermal budget of the RTA1 was fixed for all the samples, any change in the θ-Ni_2Si thickness is representative of a change in kinetic of the θ-Ni_2Si formation.

Fig. 4.a shows that the thickness of the θ phase is the lowest for the reference without PAI. For production environment samples, it increases for the 2.5, 6 and 9 nm a-Si and reaches a maximum of 9.8 nm of θ from 11 nm of a-Si. The slight variation observed for the R&D environment samples are attributed to the intrinsic mismatch between equipment and process. For both series

of samples, these different stages show that the kinetics of θ formation is faster when the NiPt reacts with a-Si than with c-Si. Indeed, the position of the silicide growth front related to the amorphous thicknesses vary for each sample. The θ phase grows only on c-Si for the reference sample. It grows first on a-Si and then on c-Si for 2.5 and 6 nm and 9 nm. For the three highest a-Si thicknesses, θ grows only on a-Si since the a-Si thickness is superior to the silicon thickness consumed to form the θ phase. The Si consumed is calculated from the silicide thickness, according to the conservation theory of matter. Thereby about 6.5 nm of Si is consumed for 9.5 nm of θ. The θ growth rate is thus faster on a-Si than on c-Si.

Fig. 4.b shows that the sheet resistance for the post RTA2 samples slightly decreases with increasing the a-Si thickness. The resistivity of the NiSi film was calculated using the simple expression, $\rho = h * R_s$ from the sheet resistance, R_s, and the silicide thickness, h, determined by XRR (Figure. 4.a). The calculated resistivities decrease for a-Si thicknesses larger than 6 nm. For production environment samples, it goes from 30.5 µohm.cm for the reference to 28 µohm.cm for the Ge PAI sample. Similarly, it goes from 31.9 µohm.cm to 29.7 µohm.cm for the R&D environment samples. Therefore, the lowest resistivities are obtained when some a-Si is left after RTA1 and thus NiSi nucleates at the θ-Ni_2Si/a-Si interface.

4. Discussion

The in-situ XRD measurements and the thicknesses measured by XRR after RTA1 shows that the thickness of the θ phase is larger when the formation of θ occurs between the NiPt layer and the a-Si. This increase reach about 30%. The formation of a phase by reaction between a thin film and a substrate usually follows three steps: nucleation, lateral growth, and normal growth (or thickening) [18]. The thickness increase may result from a change in one or several of these phenomena. For the θ-Ni_2Si phase, the nucleation and lateral growth have not been found to be limiting and a uniform thickening was reported [7]. Therefore, the increase of the thickness measured might be due to a large driving force for the first phase formation. Indeed, if the driving force should have the strongest impact both for the nucleation and lateral growth, it should also influence the normal growth [19].

Fig. 5 shows the estimated energy changes associated to the formation of θ-Ni_2Si and NiSi in the case of c-Si or a-Si and corresponds to a cut for 10%Pt at 390°C of the Gibbs energy 3D plot. It has been established using the following approximations (a) the Gibbs energies for θ-Ni_2Si and NiSi were calculated assuming an ideal solution between the Ni silicide and the Pt silicide, a Pt concentration of 10%Pt and using the Gibbs energies for the Ni-Si system assessed by Miettinen [20] (b) the Gibbs energy for a-Si was approximated by the one of liquid Si (about 30 kJ/at.gram [21]). As the a-Si phase is less stable than the c-Si phase, the free energy of the a-Si layer ($G_{a\text{-}Si}$) is higher than the free energy of the c-Si layer ($G_{c\text{-}Si}$) [21]. *Fig. 5* shows that this leads to a higher driving force (ΔG) for nucleation of θ-Ni_2Si on a-Si ($\Delta G_a^{\theta-Ni_2Si}$) than on c-Si ($\Delta G_c^{\theta-Ni_2Si}$). Indeed, accordingly to the above approximations, the driving force is increased from $\Delta G_c^{\theta-Ni_2Si} \sim -42$ kJ/at.gram on c-Si to $\Delta G_a^{\theta-Ni_2Si} \sim -52$ kJ/at.gram on a-Si (Note that an accurate determination of these driving forces would require the knowledge of the Gibbs energies for the ternary system). As the driving force for nucleation that is also involved in the lateral growth [12] is larger for a-Si than for c-Si, these two phenomena should even play a smaller role in the case of a-Si. The growth of θ-Ni_2Si should thus be controlled by its thickening that is given by Eq.1 [22].

$$\frac{dL}{dt} = \frac{D_{Ni}}{k_B T}\,\frac{\Delta\mu}{L} = \frac{D_{Ni}}{k_B T}\,\frac{\Delta G}{x_{Ni}\,L} \quad (1)$$

Where D_{Ni} is the diffusion coefficient of Ni in the growing phase, L is the phase thickness, $\Delta\mu$ is the variation of chemical potential across the growing phase. $\Delta\mu$ is proportional to the driving force ΔG trough the inverse of the atomic fraction of Ni, x_{Ni}.

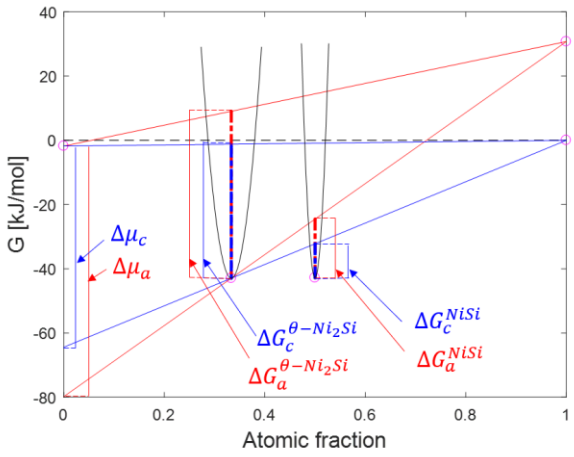

Fig. 5. Estimated changes in driving force (ΔG), and in chemical potential (Δμ) that depends on the silicon crystallinity (a-Si versus c-Si) for the θ-Ni_2Si and NiSi phase formation.

As the driving force is stronger for a-Si, the Ni atoms will migrate faster toward the θ/a-Si interface than toward the θ/c-Si resulting of a faster growth rate. Indeed, $\Delta G_a^{\theta-Ni_2Si}$ should be about 24% higher than $\Delta G_c^{\theta-Ni_2Si}$, leading to an increase in growth rate of the same percentage considering Eq. 1. The change in driving force may thus account ~~partly~~ for the larger thickness measured for a-Si (about 30% increase). Another factor than can contribute to the larger thickness can be the change in grain size since the grain boundary diffusion is preponderant in thin film [23].

Concerning NiSi, our results show that NiSi has higher roughness, lower resistivity, and forms at lower temperature when there are still some a-Si after the growth of θ. Recently El Kousseifi et al evidence that the formation of NiSi by reaction between θ and c-Si for 10nm $Ni_{0.9}Pt_{0.1}$ film is controlled by nucleation and lateral growth. They found a time (or temperature for non-isothermal heat treatment) delay between the end of θ-Ni_2Si growth and the appearance of NiSi that was attributed to the nucleation of NiSi [11]. Furthermore, they observed NiSi precipitates at the θ-Ni_2Si/c-Si interface that are representative of lateral growth [24]. Their findings allow concluding that the growth of NiSi is controlled by nucleation and lateral growth for the 10 nm $Ni_{0.9}Pt_{0.1}$ reaction with c-Si. As the same thickness and content of Pt was used in our study, the formation of NiSi should be controlled by the same mechanisms and the possible change induced by the a-Si will be now examined.

The decrease of the nucleation temperature and time delay between the $Ni_{0.9}Pt_{0.1}$ total consumption and NiSi nucleation observed for a-Si (Fig. 2) can be explained by a decrease in nucleation barrier. Indeed, Eq.2, taken from the classical nucleation theory, states the direct dependence of the nucleation barrier (ΔG*) on the variation of the interfaces energies (Δσ) and the driving force (ΔG) of the newly formed phase.

$$\Delta G^* \propto \frac{(\Delta\sigma)^3}{(\Delta G)^2} \quad (2)$$

As illustrated by the schematic on *Fig. 5*, the driving force increases if the NiSi nucleates at the θ/a-Si interface ($\Delta G_c^{NiSi} \sim -11$ kJ/at.gram) compared to the NiSi nucleation at the θ/c-Si interface ($\Delta G_a^{\mathrm{NiSi}} \sim -18$ kJ/at.gram). This increase in driving force can lower the nucleation barrier and in turn reduced time delay and nucleation temperature.

The presence of a-Si for the nucleation of NiSi can also lead the change in the interfaces energies (Δσ) that can be written as follows:

$$\Delta\sigma = \sigma_{NiSi/Si} + a_1\sigma_{NiSi/\theta} - a_2\sigma_{\theta/Si} - a_3\sigma_{GB} \quad (3)$$

Where $\sigma_{\mathrm{NiSi}/Si}$ and $\sigma_{\mathrm{NiSi}/\theta}$ are the energies of the newly created interfaces NiSi/Si and NiSi/θ respectively and $\sigma_{\theta/\mathrm{Si}}$ and σ_{GB} are the energies of the vanishing θ/Si interface and grain boundaries, respectively. It was assumed that nucleation occurs at the junction between a grain boundary and the substrate as shown in *Fig. 6*. In Eq.3, the lowest interfacial energy for the case of c-Si should be the θ/Si one since θ can grow in epitaxy on c-Si [6]. When passing from c-Si to a-Si, this interfacial energy should change to a large extent since the epitaxy is not possible on a-Si. The other interfacial energies involved in Eq. 3 (newly NiSi/Si interface and the vanishing grain boundaries) should be less sensitive to the change from c-Si to a-Si . Overall, Δσ should be lower with a-Si and contributes also to lower the nucleation barrier.

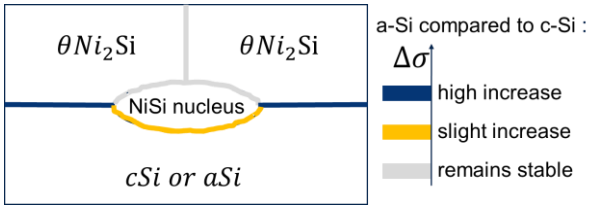

Fig. 6. Schematic showing interface energies (Δσ) evolution depending on the silicon crystallinity.

Therefore, if NiSi nucleates at the θ/a-Si interface, both the driving force and the variation of the interfaces energies implies a decrease of the nucleation barrier and thus an easier nucleation of NiSi.

In accordance with the work of Lachal et al [13], the resistivity of the silicide decreases with the a-Si thickness. There is also a slight increase of the resistivity for the thicker a-Si thicknesses (Fig. 4.b). The resistivity of NiSi should depend on the microstructure (thickness, grain size, grain boundaries, roughness) of the NiSi film that results from the formation mechanisms. Indeed, the film resistivity depends on the film thickness and on the grain boundary number and nature accordingly to the Fuchs-Sondheimer model [25,26] and the Mayadas-Shatzkes model [27,28] respectively. As the formation mechanisms leading to the film microstructure have been identified to be mainly nucleation and lateral growth, the change in resistivity may be linked to the modification induced by the a-Si on these mechanism formations of NiSi. In particular, the increase in kinetics of formation with the increasing a-Si thickness leads to an increase in silicide thickness and thus a decrease in resistivity accordingly to the Fuchs-Sondheimer model [25,26]. Moreover the position of the a-Si/c-Si interface related to the silicide nucleation and lateral growth should play a role in the NiSi microstructure. On one hand, as discussed above, the presence of a-Si allows to decrease the nucleation barrier leading to an easier nucleation of NiSi. This should lead to a higher density of nuclei at the interface except if the number of nucleation site is fixed (for example at triple junction between two θ grains). A higher density of nucleation will lead to a higher number of NiSi grains and thus a higher density of grain boundaries. As grain boundaries are expected to increase the resistance of the layer, this should lead to an increase in resistivity [27,28]. On the other hand, the increase in driving force for NiSi (*Fig. 5*) is also expected to increase the kinetics of lateral growth [10]. A faster lateral growth on a-Si should lead to less grains since the time to nucleate new grains will be reduced. As the resistivity is decreased when a-Si is still present after the formation of θ-Ni_2Si (Fig. 4), the overall effect of a-Si on nucleation and lateral growth of NiSi should be a decrease of grain boundaries.

The roughness of the silicide layer is also a parameter that could influence its resistivity. Indeed, for a rough sample, the resistivity will be artificially increased as illustrated with Fig. 7. A rough layer means that the thickness is smaller in some places and that the electrons path is reduced through a lower effective thickness. Moreover, the increase of surface and/or interface linked to the roughness may also increase the resistivity of the film [27–29].

$$\rho = R_s * e$$

ρ : Resistivity (µohm.cm)

R_S : Sheet Resistance (ohm/sq)

e : Effective thickness that contributes to the resistivity

e : Measured thickness

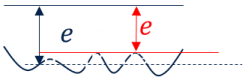

Fig. 7. Schematic impact of the roughness on the resistivity

According to the XRR spectra, the NiSi roughness is deteriorated for the larger thicknesses of the a-Si layer. Therefore, it could not explain the decrease resistivity since the roughness should increase artificially the value of the resistivity. This point confirms that the grain size change constitutes a clue to explain the resistivity variations since it cannot be explained by the roughness variation.

However, even if the resistivity stays lower than the reference, a slight increase of the resistivity is observed for the two thicker a-Si. It can be related to the higher roughness qualitatively observed with the XRR spectra. This higher roughness could be due to the damage induced by the PAI. Indeed, if the a-Si layer is too deep, the silicide growth front does not pass through the a-Si/c-Si interface and damage area resulting of a rough interface which increased artificially the resistivity. Another possibility is the formation of $NiSi_2$ that is possible at low temperature on a-Si [30]. However, this formation was not observed in our samples by TEM or XRD.

.

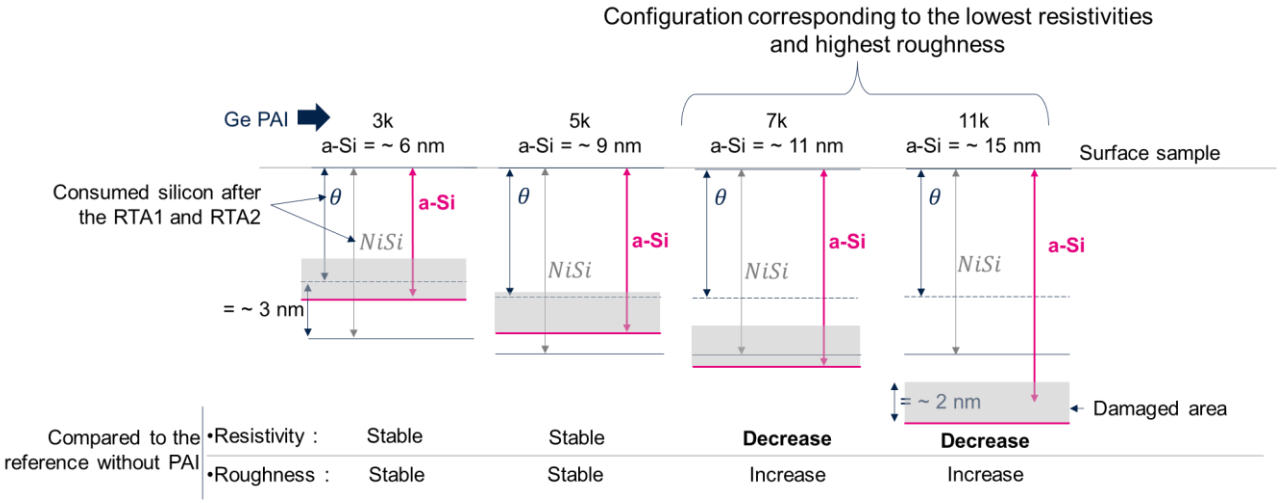

Fig. 8. Schematic representing the position of the a-Si/c-Si interface related with the silicide growth front.

Fig. 8 is a summary of the different situations regarding the silicon consumed and the a-Si thickness. Our results show that these situations influence the silicide formation and properties. To summarize, if the amorphous thickness is not deep enough, the NiSi nucleation is not impacted by the amorphous substrate, thus the grain diameter remains constant, and the resistivity does not decrease. However, if the amorphous thickness is too deep or the damage area too large, the roughness of the silicide is deteriorated

Therefore, as illustrated on the schematic Fig. 8, a good compromise is reached if NiSi nucleates at the θ/a-Si interface and if the silicide growth front passes through the damaged area. This configuration is not easy to reach since the thickness between the silicon consumed after the RTA1 and after the RTA2 is about 3 nm thick and the damaged layer is about 2 nm thick. Therefore, for the same decrease of the resistivity, the roughness could be less deteriorated if the damage area is reduced. A simple solution to reduce the thickness of the damaged area would be to modify the Ge PAI condition by increasing the dose or using low temperature implantation.

5. Conclusion

The position of the a-Si/c-Si interface compared to the silicide growth front is determined after the first and second anneal from which the θ-Ni_2Si and NiSi phase grows, respectively. therefore, the environment of the θ-Ni_2Si growth rate and NiSi nucleation site is clearly identified for each sample. Kinetics and properties variations induced by the amorphous layer are studied. First, the θ-Ni_2Si growth rate is faster on a-Si than on c-Si. The change in driving force induced by the amorphous layer is considered to explain the increase of the θ-

Ni_2Si growth rate. Then, the decrease of the nucleation temperature and time delay between the

$Ni_{0.9}Pt_{0.1}$ total consumption and NiSi nucleation observed for a-Si is explained by a decrease in nucleation barrier. Finally, the silicide properties are studied. The resistivity of the silicide decreases with the a-Si thickness. It is put forward that the resistivity is lowered when a-Si is still present after the θ-Ni_2Si formation and thus NiSi nucleation and lateral growth occurs at the θ-Ni_2Si/a-Si interface. There is also a slight increase of the resistivity for the thicker a-Si thicknesses attributed to the increase roughness caused by the rough and thick damaged area. Therefore, a good compromise is reached if NiSi nucleates at the θ/a-Si interface and if the silicide growth front passes clearly through the damaged area.

Acknowledgments

This work was supported by the STMicroelectronics-Leti alliance program and the French National Research Agency (ANR) under the "Investissements d'avenir" programs: ANR 10-EQPX-0030 (EQUIPEX FDSOI 11). The authors would like to thank E. Ghegin and Y. Escarabajal for process assistance on samples preparation, E. Nolot, C. Perrin-Pellegrino and A. Michallet for technical assistance on samples characterizations, K. Dabertrand, A. Valery and P. Benigni for fruitful discussions.

References

[1] C. Lavoie, F.M. d'Heurle, C. Detavernier, C. Cabral Jr., Towards implementation of a nickel silicide process for CMOS technologies, Microelectronic Engineering. 70 (2003) 144–157. https://doi.org/10.1016/S0167-9317(03)00380-0.

[2] D. Mangelinck, J.Y. Dai, J.S. Pan, S.K. Lahiri, Enhancement of thermal stability of NiSi films on (100)Si and (111)Si by Pt addition, Applied Physics Letters. 75 (1999) 1736–1738. https://doi.org/10.1063/1.124803.

[3] C. Detavernier, C. Lavoie, Influence of Pt addition on the texture of NiSi on Si(001), Applied Physics Letters. 84 (2004) 3549. https://doi.org/10.1063/1.1719276.

[4] T. Sonehara, A. Hokazono, H. Akutsu, T. Sasaki, H. Uchida, M. Tomita, H. Tsujii, S. Kawanaka, S. Inaba, Y. Toyoshima, Contact resistance reduction of Pt-incorporated NiSi for continuous CMOS scaling ～ Atomic level analysis of Pt/B/As distribution within silicide films ～, in: 2008 IEEE International Electron Devices Meeting, 2008: pp. 1–4. https://doi.org/10.1109/IEDM.2008.4796851.

[5] O. Weber, E. Josse, F. Andrieu, A. Cros, E. Richard, P. Perreau, E. Baylac, N. Degors, C. Gallon, E. Perrin, S. Chhun, E. Petitprez, S. Delmedico, J. Simon, G. Druais, S. Lasserre, J. Mazurier, N. Guillot, E. Bernard, R. Bianchini, L. Parmigiani, X. Gerard, C. Pribat, O. Gourhant, F. Abbate, C. Gaumer, V. Beugin, P. Gouraud, P. Maury, S. Lagrasta, D. Barge, N. Loubet, R. Beneyton, D. Benoit, S. Zoll, J.-D. Chapon, L. Babaud, M. Bidaud, M. Gregoire, C. Monget, B. Le-Gratiet, P. Brun, M. Mellier, A. Pofelski, L.R. Clement, R. Bingert, S. Puget, J.-F. Kruck, D. Hoguet, P. Scheer, T. Poiroux, J.-P. Manceau, M. Rafik, D. Rideau, M.-A. Jaud, J. Lacord, F. Monsieur, L. Grenouillet, M. Vinet, Q. Liu, B. Doris, M. Celik, S.P. Fetterolf, O. Faynot, M. Haond, 14nm FDSOI technology for high speed and energy efficient applications, in: 2014 Symposium on VLSI Technology (VLSI-Technology): Digest of Technical Papers, 2014: pp. 1–2. https://doi.org/10.1109/VLSIT.2014.6894343.

[6] F. Panciera, D. Mangelinck, K. Hoummada, M. Texier, M. Bertoglio, A. De Luca, M. Gregoire, M. Juhel, Direct epitaxial growth of θ-Ni2Si by reaction of a thin Ni(10 at.% Pt) film with Si(1 0 0) substrate, Scripta Materialia. 78–79 (2014) 9–12. https://doi.org/10.1016/j.scriptamat.2014.01.010.

[7] M. Putero, L. Ehouarne, E. Ziegler, D. Mangelinck, First silicide formed by reaction of Ni(13%Pt) films with Si(1 0 0): Nature and kinetics by in-situ X-ray reflectivity and diffraction, Scripta Materialia. 63 (2010) 24–27. https://doi.org/10.1016/j.scriptamat.2010.02.040.

[8] F. Panciera, K. Hoummada, C. Perrin, M. El Kousseifi, R. Pantel, M. Descoins, M. Gregoire, M. Juhel, D. Mangelinck, Ni(Pt)-silicide contacts on CMOS devices: Impact of substrate nature and Pt concentration on the phase formation, Microelectronic Engineering. 120 (2014) 34–40. https://doi.org/10.1016/j.mee.2013.12.016.

[9] M. El Kousseifi, K. Hoummada, M. Bertoglio, D. Mangelinck, Selection of the first Ni silicide phase by controlling the Pt incorporation in the intermixed layer, Acta Materialia. 106 (2016) 193–198. https://doi.org/10.1016/j.actamat.2016.01.004.

[10] F.A. Geenen, E. Solano, J. Jordan-Sweet, C. Lavoie, C. Mocuta, C. Detavernier, The influence of alloying on the phase formation sequence of ultra-thin nickel silicide films and on the inheritance of texture, Journal of Applied Physics. 123 (2018) 185302. https://doi.org/10.1063/1.5022070.

[11] M. El Kousseifi, K. Hoummada, F. Panciera, C. Lavoie, D. Mangelinck, Nucleation and lateral growth kinetics of the NiSi phase at the epitaxial θ-Ni2Si/Si interface, Acta Materialia. 198 (2020) 100–110. https://doi.org/10.1016/j.actamat.2020.07.062.

[12] D. Mangelinck, M. El Kousseifi, K. Hoummada, F. Panciera, T. Epicier, Lateral growth of NiSi at the θ-Ni2Si/Si(100) interface: Experiments and modelling, Microelectronic Engineering. 199 (2018) 45–51. https://doi.org/10.1016/j.mee.2018.07.014.

[13] K. van Stiphout, F.A. Geenen, N.M. Santos, S.M.C. Miranda, V. Joly, J. Demeulemeester, C. Mocuta, C.M. Comrie, C. Detavernier, L.M.C. Pereira, K. Temst, A. Vantomme, Ion beam modification of the Ni-Si solid-phase reaction: The influence of substrate damage and nitrogen impurities introduced by ion implantation, J. Phys. D: Appl. Phys. 54 (2020) 015307. https://doi.org/10.1088/1361-6463/abb046.

[14] L. Lachal, Effects of Pre-amorphization Thickness and Carbon Implantation on NiPt/Si Silicidation Process, in: 2018.

[15] A.S. Ozcan, D. Wall, J. Jordan-Sweet, C. Lavoie, Effects of temperature dependent pre-amorphization

implantation on NiPt silicide formation and thermal stability on Si(100), Appl. Phys. Lett. 102 (2013) 172107. https://doi.org/10.1063/1.4801928.
[16] R. Yang, N. Su, P. Bonfanti, J. Nie, J. Ning, T.T. Li, Advanced in situ pre-Ni silicide (Siconi) cleaning at 65nm to resolve defects in NiSix modules, Journal of Vacuum Science & Technology B. 28 (2010) 56–61. https://doi.org/10.1116/1.3271334.
[17] D. Mangelinck, K. Hoummada, Effect of stress on the transformation of Ni2Si into NiSi, Applied Physics Letters. 92 (2008) 254101. https://doi.org/10.1063/1.2949751.
[18] D. Mangelinck, K. Hoummada, F. Panciera, M. El Kousseifi, I. Blum, M. Descoins, M. Bertoglio, A. Portavoce, C. Perrin, M. Putero, Progress in the understanding of Ni silicide formation for advanced MOS structures, Physica Status Solidi A-Applications and Materials Science. 211 (2014) 152–165. https://doi.org/10.1002/pssa.201300167.
[19] D. Mangelinck, Mechanisms of Silicide Formation by Reactive Diffusion in Thin Films, Diffusion Foundations. 21 (2019) 1–28. https://doi.org/10.4028/www.scientific.net/DF.21.1.
[20] J. Miettinen, Thermodynamic description of the Cu–Ni–Si system in the copper-rich corner above 700 ∘C, Calphad. 29 (2005) 212–221. https://doi.org/10.1016/j.calphad.2005.08.001.
[21] J.-F. Mercure, R. Karmouch, Y. Anahory, S. Roorda, F. Schiettekatte, Dependence of the structural relaxation of amorphous silicon on implantation temperature, Phys. Rev. B. 71 (2005) 134205. https://doi.org/10.1103/PhysRevB.71.134205.
[22] D. Mangelinck, T. Luo, C. Girardeaux, Reactive diffusion in the presence of a diffusion barrier: Experiment and model, Journal of Applied Physics. 123 (2018) 185301. https://doi.org/10.1063/1.5023578.
[23] T. Barge, P. Gas, F.M. d'Heurle, Analysis of the diffusion controlled growth of cobalt silicides in bulk and thin film couples, Journal of Materials Research. 10 (1995) 1134–1145. https://doi.org/10.1557/JMR.1995.1134.
[24] M. El Kousseifi, K. Hoummada, T. Epicier, D. Mangelinck, Direct observation of NiSi lateral growth at the epitaxial θ-Ni2Si/Si(1 0 0) interface, Acta Materialia. 99 (2015) 1–6. https://doi.org/10.1016/j.actamat.2015.07.062.
[25] K. Fuchs, The conductivity of thin metallic films according to the electron theory of metals, Mathematical Proceedings of the Cambridge Philosophical Society. 34 (1938) 100–108. https://doi.org/10.1017/S0305004100019952.
[26] E.H. Sondheimer, The mean free path of electrons in metals, Advances in Physics. 1 (1952) 1–42. https://doi.org/10.1080/00018735200101151.
[27] A.F. Mayadas, Electrical-Resistivity Model for Polycrystalline Films: the Case of Arbitrary Reflection at External Surfaces, Phys. Rev. B. 1 (1970) 1382–1389. https://doi.org/10.1103/PhysRevB.1.1382.
[28] L. Moraga, C. Arenas, R. Henriquez, S. Bravo, B. Solis, The electrical conductivity of polycrystalline metallic films, Physica B: Condensed Matter. 499 (2016) 17–23. https://doi.org/10.1016/j.physb.2016.07.001.
[29] R.S. Smith, E.T. Ryan, C.-K. Hu, K. Motoyama, N. Lanzillo, D. Metzler, L. Jiang, J. Demarest, R. Quon, L. Gignac, C. Breslin, A. Giannetta, S. Wright, An evaluation of Fuchs-Sondheimer and Mayadas-Shatzkes models below 14nm node wide lines, AIP Advances. 9 (2019) 025015. https://doi.org/10.1063/1.5063896.
[30] C.-D. Lien, M.-A. Nicolet, S.S. Lau, Low Temperature Formation of Nisi2 from Evaporated Silicon, Physica Status Solidi (a). 81 (1984) 123–128. https://doi.org/10.1002/pssa.2210810111.